Coexistence of Room Temperature Magneto-Chiral Dichroism and Magneto-Electric Coupling in a Chiral Nanomagnet

Langit Cahya Adi,[a] Maxime Aragon-Alberti,[a,b] Geert L.J.A. Rikken,[a] Cyrille Train,[a] Jérôme Long,[b],[c]* Matteo Atzori[a],*

[a] Laboratoire National des Champs Magnétiques Intenses (LNCMI), CNRS, Univ. Grenoble Alpes, INSA Toulouse, Univ. Toulouse Paul Sabatier, EMFL, F-38042 Grenoble – France.

[b] Institut Charles Gerhardt Montpellier, UMR 5253, Université de Montpellier, ENSCM, CNRS, Place E. Bataillon, F-34095 Montpellier – France.

[c] Institut Universitaire de France (IUF), 1 rue Descartes, 75231 Paris – France.

Corresponding authors:

Dr. Matteo Atzori, matteo.atzori@lncmi.cnrs.fr

Prof. Jérôme Long, jerome.long@umontpellier.fr

SUPPLEMENTARY INFORMATION

EXPERIMENTAL SECTION

Synthesis. The samples were prepared and characterized according to the published procedures.[S1] The ligand 6,6'-((1E,1'E)-(((1*R*,2*R*)-1,2-diphenylethane-1,2-diyl)bis(azaneylylidene))bis(methane ylylidene))bis(2-methoxyphenol) (*R,R*-H_2L) or 6,6'-((1E,1'E)-(((1S,2S)-1,2-diphenylethane-1,2-diyl)bis(azaneylylidene))bis(methaneylylidene))bis(2-methoxyphenol) (*S,S*-H_2L) have been synthesized according to the published procedure.[S1]

The stoichioemetric reaction between *R,R*-H_2L (0.1 mmol, 0.046 g), $Zn(OAc)\cdot 2H_2O$ (0.1 mmol, 0.022 g) and $Yb(NO_3)_3\cdot 5H_2O$ (0.1 mmol, 0.045 g) in 10 mL of a methanol/acetonitrile (4:1) mixture, gives a clear yellow solution. Slow vapour diffusion of diethyl-ether into the yellow solution leads to the formation of block-shaped yellow crystals of **1-(*R*,*R*)** suitable for MChD measurements. The same procedure was used to obtain **1-(*S*,*S*)** starting from *S,S*-H_2L.

Magnetic measurements. Magnetic measurements as a function of temperature were performed in the 2.0-300 K temperature range with an applied magnetic field of 1.0 T on a polycrystalline sample of **1-*(R,R)*** by using a *Quantum Design MPMS3-VSM-SQUID* magnetometer. The microcrystalline sample was finely grounded and pressed in the form of a pellet to avoid microcrystalline orientations. Magnetization measurements as a function of an externally applied magnetic field were collected on the same sample at T = 4.0 K with magnetic fields up to +7 T. Susceptibility data were corrected for the sample holders previously measured in the same conditions and for the diamagnetic contributions as by using Pascal's constant tables.[S2]

Magneto-Chiral Dichroism Spectroscopy. Magneto-Chiral Dichroism spectra were recorded with a home-made multichannel MChD spectrometer operating in the visible and near infrared spectral window (400−1600 nm) between 4.0 and 290 K with an alternating magnetic field $\boldsymbol{B}$ up to ±2 T. MChD spectra were acquired on single crystals of enantiopure **1-*(R,R)*** and **1-(*S,S*)**. The samples were mounted on a titanium sample holder over a 0.5 mm hole diameter centred with respect to a 1.0 mm diameter collimated beam. Measurements were performed in the 4.0−290 K range with an alternating magnetic field $\boldsymbol{B}$ = ±1.0 T and frequency Ω = 0.04 Hz. MChD spectra as a function of the magnetic field were recorded at T = 4.0 K for alternating magnetic fields of different amplitudes (0.0-2.0 T). Unpolarized light was provided by a broadband Energetiq – Hamamatsu Laser Driven Light Sources (EQ-99X-FC-S or EQ-77X-FC-S). MChD spectra were obtained at each temperature/magnetic field value by collecting, on average, 30.000 spectra with an integration time of 25 ms. The spectra were collected with a high resolution/high sensitivity Optosky detector equipped with a thermoelectric cooled sensor operating in the 200−1000 nm spectral region with an analogic/digital convertor of 16 bits. Each spectrum was correlated to a

specific magnetic field value by a dual channel digitizer (Picoscope 5000B) acquiring simultaneously triggers from the spectrometer and the magnetic field from a calibrated Hall effect sensor (Lakeshore) placed in proximity of the sample. Data were then post-processed as a synchronous detection with a specific MatLab routine to obtain the MChD spectra.

The MChD dissymmetry factor g_{MChD} is defined as follows:

$$g_{MChD} = \frac{\Delta A_{MChD}}{A\,\boldsymbol{B}} \qquad \text{(eq. S1)}$$

where ΔA_{MChD} is the differential absorption coefficient between the light absorption collected under a magnetic field parallel and antiparallel oriented with respect to the light wavevector $\boldsymbol{k}$, A is the effective absorption coefficients of the electronic transitions at zero field and $\boldsymbol{B}$ is the applied magnetic field intensity.

Theoretical Calculations.

CASSCF calculations were performed with ORCA 5.0 software[S3,S4] using the crystallographic structures without any structural geometry optimization. Tolerance for energy convergence is fixed at 10^{-7} Eh. An active space considering the seven 4f orbitals with 13 electrons CAS (13, 7) for all the doublets (7 roots) was considered. To account for dynamic correlation effects and provide a more accurate picture of the CF splitting, second-order N-Electron perturbation theory (NEVPT2) calculations were performed on top of the CASSCF calculations. The def2 Ahlrichs basis sets were used: DKH-DEF2-TZVP for all atoms, except for Yb for which SARC2-DKH-QZVP basis set was employed. The AUTOAUX feature was employed to automatically generate auxiliary basis sets within the RIJCOSX approximation to speed up the calculations. Finally, the SINGLE_ANISO program[S4] implemented in ORCA was utilized to obtain detailed information about magnetic relaxation.

ADDITIONAL FIGURES AND TABLES

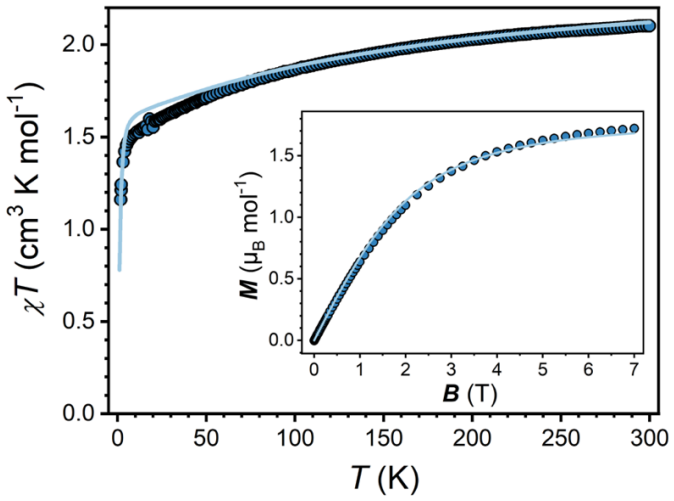

Figure S1. Temperature dependence (2-300 K) of the molar magnetic susceptibility times the temperature (χT) under an applied static magnetic field $\boldsymbol{B}$ = 1.0 T for a finely grounded microcrystalline sample of **1-*(R,R)***. Inset shows the magnetization curve as a function of the magnetic field intensity at T = 4.0 K. The solid lines account for the calculated values from theoretical calculations downscaled by about 10% with respect to the experimental data.

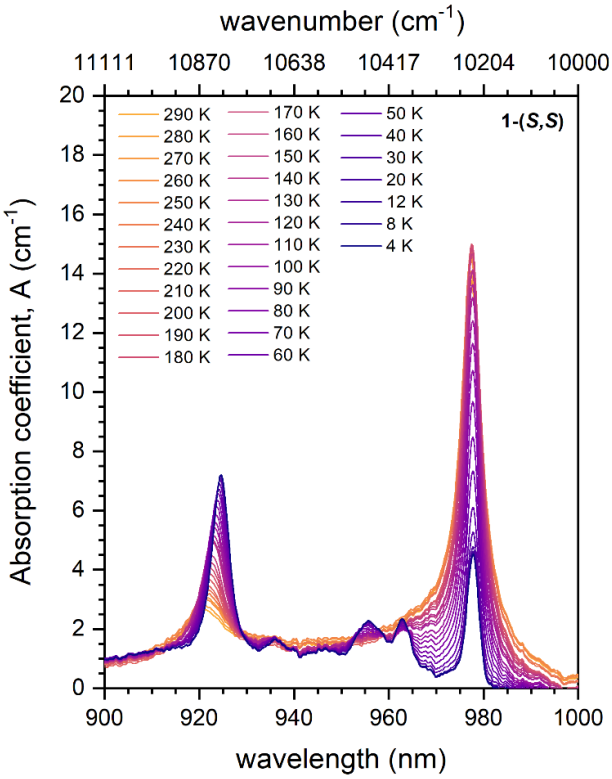

Figure S2. Thermal variation of the absorption coefficient for a single crystal of **1-(*R,R*)** (k⊥(0,-1,1) in the 900-1000 nm range.

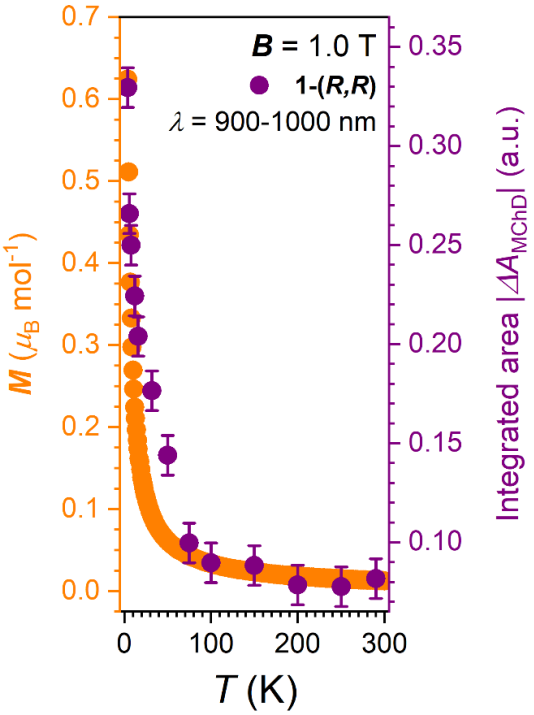

Figure S3. Temperature dependence of ΔA_{MChD} (integrated absolute area of the overall $^2F_{7/2} \leftarrow {}^2F_{5/2}$ multiplet λ = 900-1000 nm) compared to the magnetization data recorded on a finely grounded microcrystalline sample of **1-*(R,R)*** under the same applied magnetic field ***B*** = 1.0 T.

Table S1. *Ab initio* calculated energies, ***g***-tensor main values of the ground doublet and the nth KD doublet for the ground multiplet J = 7/2 obtained for **Yb1** of **1-*(R,R)***.

CASSCF					
KD	**Energy (cm^{-1})**	g_x	g_y	g_z	**Wavefunction (only components with > 20 % are given)**
0	0	0.48911927	0.80066600	7.56304043	94.6.% |±7/2>
1	197	4.54825284	3.52712890	1.19587360	72.9% |±5/2>
2	437	0.98668224	1.27830005	4.30320799	46.0% |±3/2>;28.9% |±1/2>;22.2% |±5/2>
3	575	0.41755301	0.55279656	7.45859501	61.4% |±1/2>; 34.1% |±3/2>
NEVPT2					
KD	**Energy (cm^{-1})**	g_x	g_y	g_z	**Wavefunction (only components with > 20 % are given)**
0	0.00	0.55125575	0.90915232	7.51638665	94.0.% |±7/2>
1	224	4.76473305	2.99164483	1.02756954	76.9% |±5/2>
2	558	1.48328089	1.60992603	4.05250395	51.9% |±3/2>;26.7% |±1/2>
3	713	0.31826735	0.43113190	7.49285237	64.4% |±1/2>; 31.4% |±3/2>

Table S2. *Ab initio* calculated energies of the ground doublet and the nth KD doublet for the multiplet J = 5/2 obtained for **Yb1** of **1-*(R,R)***.

CASSCF		
KD	**Energy (cm^{-1})**	**Energy rescaled (cm^{-1})**
0'	10143	0
1'	10381	238
2'	10636	493
NEVPT2		
KD	**Energy (cm^{-1})**	**Energy rescaled (cm^{-1})**
0'	10156	0
1'	10452	296
2'	10777	621

Table S3. *Ab initio* calculated energies, *g*-tensor main values of the ground doublet and the nth KD doublet for the ground multiplet J = 7/2 obtained for **Yb2** of **1-*(S,S)***.

CASSCF					
KD	**Energy (cm^{-1})**	g_x	g_y	g_z	**Wavefunction (only components with > 20 % are given)**
0	0	0.39260608	0.75718215	7.57227107	94.4% |±7/2>
1	198	4.52627306	3.64928336	1.07890249	72.8% |±5/2>
2	420	0.67414124	1.25857337	4.48299877	45.4% |±3/2>;29.4% |±1/2>;22.4% |±5/2>
3	560	0.51891643	0.62553761	7.42920966	60.5% |±1/2>; 34.6% |±3/2>
NEVPT2					
KD	**Energy (cm^{-1})**	g_x	g_y	g_z	**Wavefunction (only components with > 20 % are given)**
0	0	0.39571912	0.76796636	7.56438092	94.1% |±7/2>
1	231	4.78619781	3.04355095	0.91611097	78.7% |±5/2>
2	542	1.12311714	1.88266121	4.24414673	50.9% |±3/2>;29.0% |±1/2>
3	701	0.43447747	0.49925249	7.46083346	62.6% |±1/2>; 33.0% |±3/2>

Table S4. *Ab initio* calculated energies of the ground doublet and the nth KD doublet for the multiplet J = 5/2 obtained for **Yb2** of **1-*(S,S)***.

CASSCF		
KD	**Energy (cm^{-1})**	**Energy rescaled (cm^{-1})**
0'	10144	0
1'	10375	228
2'	10621	477
NEVPT2		
KD	**Energy (cm^{-1})**	
0'	10157	0
1'	10449	291
2'	10764	607

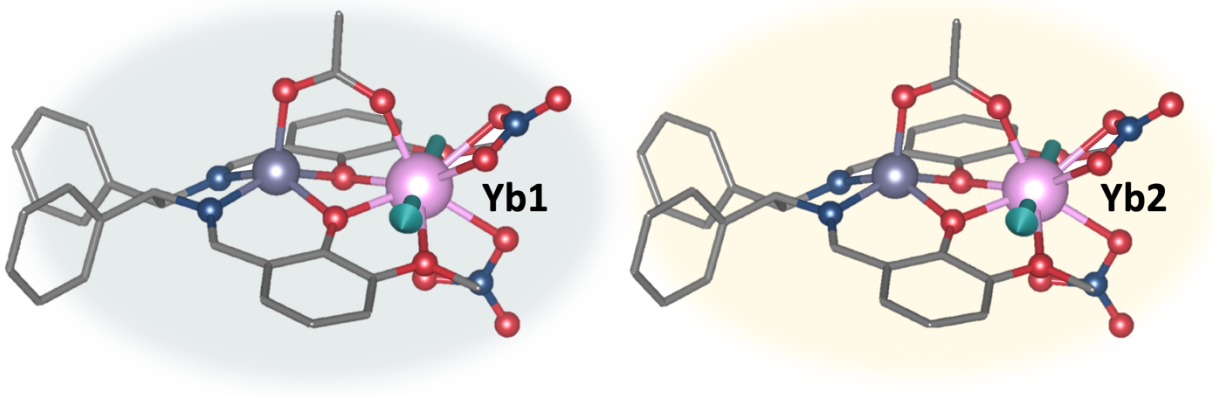

Figure S4. Orientation of the magnetic easy-axis (green arrow) related to the ground Kramers doublet (0) for the two crystallographically independent Yb^{III} ions.

SUPPORTING REFERENCES

S1. J. Long, M. S. Ivanov, V. A. Khomchenko, E. Mamontova, J.-M. Thibaud, J. Rouquette, M. Beaudhuin, D. Granier, R. A. S. Ferreira, L. D. Carlos, B. Donnadieu, M. S. C. Henriques, J. A. Paixão, Y. Guari, J. Larionova, *Science* **2020**, *367,* 671–676.

S2. G. A. Bain, J. F. Berry, *J. Chem. Educ.* **2008**, *85*, 532.

S3. F. Neese, *Wiley Interdiscip. Rev. Comput. Mol. Sci.*, **2012**, *2*, 73-78.

S4. F. Neese, *Wiley Interdiscip. Rev. Comput. Mol. Sci.*, **2022**, *12*, e1606.

S5. L. Ungur and L. F. Chibotaru, *SINGLE_ANISO Program* **2006-2013**.